JGR Solid Earth

RESEARCH ARTICLE
10.1029/2018JB016201

Rates of Dynamic Recrystallization in Geologic Materials

A. J. Cross[1,2] and **P. Skemer**[1]

[1]Department of Earth and Planetary Sciences, Washington University in St. Louis, St. Louis, MO, USA, [2]Department of Earth and Environmental Sciences, University of Pennsylvania, Philadelphia, PA, USA

Abstract Grain size reduction via dynamic recrystallization (DRX) is intimately related to the softening of crystalline materials under an applied stress, and plays a role in numerous geodynamic processes that involve strain-weakening feedbacks. Despite its importance, few studies have provided empirical constraints on the rates of DRX and grain size reduction. Here we examine DRX rates using the Johnson-Mehl-Avrami-Kolmogorov theory for phase transformation kinetics. Our analysis uses a compilation of published and newly-derived DRX data from experimental studies on a wide range of geologic and engineering materials. We find that DRX rates are strongly dependent on the homologous temperature at which deformation occurs, with DRX occurring over a broad range of shear strains ($0.01 < \gamma < 200$), and more rapidly with increasing homologous temperature. Moreover, the experimental data can be described by a single fit to a modified form of the Avrami equation that incorporates homologous temperature dependence, implying that, to first order, DRX rates are largely material independent. We also examine the influence of stress, deformation work rate, crystal orientation, and initial grain size on DRX rates and compare DRX data from experimental and natural conditions. Overall, we show that microstructures can evolve over long transient intervals, and provide a framework for determining DRX kinetics from empirical data, which can ultimately be incorporated into geodynamic models of grain size evolution in the Earth.

Key Points:
- Dynamic recrystallization (DRX) rates are examined for a compilation of experimental data using the Avrami theory for transformation kinetics
- DRX rates are strongly dependent on homologous temperature, with DRX occurring over a broad range of shear strains ($0.01 < \gamma < 200$)
- Experimental DRX data can be fit using a single, material-independent relationship that incorporates homologous temperature

Supporting Information:
- Supporting Information S1

Correspondence to:
A. J. Cross,
andcross@sas.upenn.edu

Citation:
Cross, A. J., & Skemer, P. (2019). Rates of dynamic recrystallization in geologic materials. *Journal of Geophysical Research: Solid Earth*, *124*. https://doi.org/10.1029/2018JB016201

Received 11 JUN 2018
Accepted 9 JAN 2019
Accepted article online 14 JAN 2019

1. Introduction

Dynamic recrystallization and recovery are fundamental processes in the crystal plastic deformation of rocks and minerals, whereby the elastic strain energy associated with linear lattice defects (i.e., dislocations) is minimized by the reorganization of those defects into low-energy configurations (Poirier & Guillopé, 1979; White, 1977). During dynamic recrystallization (DRX), strain hardening due to the accumulation of lattice defects is counteracted by both the creation and migration of grain boundaries, and the nucleation of new, strain-free recrystallized grains (e.g., Urai et al., 1986; Figure 1). In laboratory deformation experiments, the onset of DRX is often related to the onset of strain weakening (e.g., Luton & Sellars, 1969; Poliak & Jonas, 1996; Rutter, 1999), while in nature, severe grain size reduction is almost ubiquitously observed in the high-strain interiors of ductile shear zones (e.g., Linckens et al., 2015; Rutter & Brodie, 1988; Warren & Hirth, 2006; White, 1979). Thus, DRX has long been considered an essential process for the accumulation of large plastic strains in the Earth's crust and mantle (Etheridge & Wilkie, 1979; Montési & Hirth, 2003; Platt & Behr, 2011; Poirier, 1980; Tullis & Yund, 1985; White et al., 1980). More recently, it has also been argued that DRX and grain size evolution play a key role in other geodynamic phenomena, including mantle convection (Barr & McKinnon, 2007; Dannberg et al., 2017; Hall & Parmentier, 2003; Rozel, 2012), mantle plume dynamics (Korenaga, 2005), intermediate-depth earthquake nucleation (Thielmann et al., 2015), passive margin collapse (Mulyukova & Bercovici, 2018), and plate boundary formation (e.g., Bercovici & Ricard, 2012).

Numerous authors have modeled DRX from theoretical and numerical perspectives. Primarily, these approaches are rooted in the assumption that grain size evolves through a dynamic competition between grain growth and DRX (see Austin & Evans, 2007; De Bresser et al., 2001; Platt & Behr, 2011): when the rates of these processes are balanced, a steady state grain size is established. Whereas the kinetics of static grain growth are reasonably well established (Covey-Crump, 1997; Evans et al., 2001; Faul & Scott, 2006; Hiraga et al., 2010; Karato, 1989; Olgaard & Evans, 1988; Skemer & Karato, 2007; Tullis & Yund, 1982; Yoshino & Yamazaki, 2007) and are typically parameterized in the form of a normal grain growth law (Kingery et al., 1976), there are few empirical data on the rates of grain size reduction by DRX in geologic materials. Previous treatments of grain size evolution have considered the rate of DRX as a function of the dissipation of deformation work through grain boundary production (Austin & Evans, 2007, 2009;

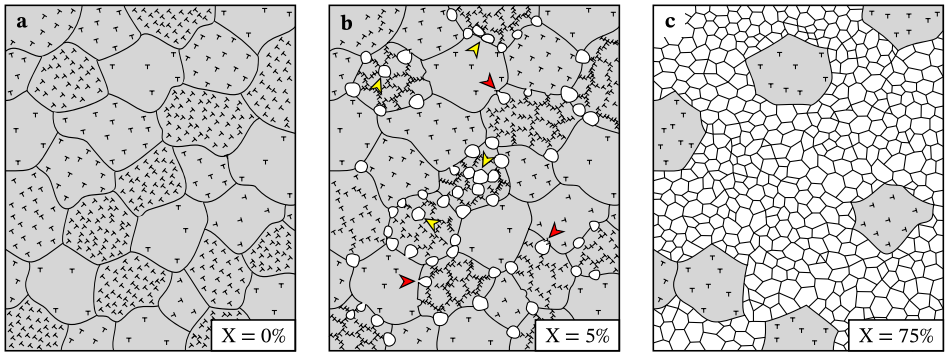

Figure 1. Schematic representation of dynamic recrystallization in a deforming polycrystal. (a) Dislocations accumulate heterogeneously under an applied stress. (b and c) High-strain relict grains (gray) are progressively consumed by the nucleation of strain-free recrystallized grains (white), formed by grain boundary bulging (red arrows) and subgrain rotation (yellow arrows) nucleation mechanisms, causing an increase in the recrystallized fraction, X.

Bercovici & Ricard, 2005; Rozel et al., 2011), the probability of grain nucleation based on the stored energy of a given grain (Jessell et al., 2005; Piazolo et al., 2002; Wenk et al., 1997), the minimization of a grain population's internal energy (Mulyukova & Bercovici, 2019), or gravitation toward a mechanistically-bounded steady-state grain size (Braun et al., 1999; Cross et al., 2015; Hall & Parmentier, 2003; Holtzman et al., 2018). However, few studies have explored the kinetics of DRX using empirical (i.e., experimental or field-based) data.

To quantify and investigate the rates and kinetics of DRX in geologic materials, we have compiled and reanalyzed published DRX data (supporting information Table S1) using the Johnson-Mehl-Avrami-Kolmogorov model, otherwise known as the JMAK or Avrami model, which describes the kinetics of phase transformations, like recrystallization, wherein a volume of material undergoes transformation by the nucleation and growth of a new phase. Originally developed for the purpose of modeling crystallization, phase transformations, and static recrystallization (Avrami, 1940; Johnson & Mehl, 1939; Kolmogorov, 1937), Avrami theory was later examined in the context of DRX by Roberts et al. (1979) and has previously been used to investigate dehydration kinetics (Llana-Fúnez et al., 2007), phase transformations (Carlson, 1983; Riedel & Karato, 1996), static grain growth (Covey-Crump, 1997), and DRX (Shigematsu, 1999; Skemer & Karato, 2008) in geologic materials. By applying Avrami kinetic theory to experimental DRX data (i.e., recrystallized fraction as a function of strain), we show that DRX rates are strongly dependent on homologous temperature and can be expressed, to first order, using a single, material-independent relationship, at least under experimental (i.e., high temperature and high strain rate) conditions.

2. Avrami Kinetics

2.1. General Form

For a material undergoing random nucleation and growth of a new phase, the transformed fraction, X, (i.e., the volume or area fraction of material occupied by the new phase) increases monotonically as a product of the nucleation rate, N, and the volume, ν, of each nucleus (formed at time, τ, and growing through time, t), integrated over the duration of the transformation, beginning at the critical time, t_c (Avrami, 1940; Farjas & Roura, 2006; Humphreys & Hatherly, 2004; Woldt, 1992):

$$X_{\mathrm{ex}}(t) = \int_{t_c}^{t} \nu(t,\tau)\, N(\tau)\, \mathrm{d}\tau \tag{1}$$

in which the volume of each nucleus is given by

$$\nu(t,\tau) = \alpha\left(\int_{\tau}^{t} G(z)\, \mathrm{d}z\right)^{m} \tag{2}$$

where α is a shape factor (e.g., $4\pi/3$ for spherical nuclei), $G(z)$ is the growth rate, and m describes the spatial dimensionality of growth (e.g., $m = 3$ for three-dimensional growth of nuclei).

Rather than giving the true transformed fraction, X, equation (1) gives the *extended volume*, X_{ex}, which is the transformed volume occupied when grains are able to grow unimpeded (i.e., without impinging on one another). To account for impingement, the transformed fraction, X, is instead given as

$$X(t) = 1 - \exp[-X_{ex}(t)] \tag{3}$$

where from the substitution of equations (1) and (2), we obtain

$$X(t) = 1 - \exp\left[-\int_{t_c}^{t} \alpha \left(\int_{\tau}^{t} G(z)\, dz\right)^{m} N(\tau)\, d\tau\right] \tag{4}$$

In general, it is assumed that the nucleation and growth rates (N and G, respectively) follow an Arrhenius-type temperature dependence, given by

$$N(t) = N_0 \exp\left(\frac{-Q_N}{RT}\right) \tag{5}$$

and

$$G(t) = G_0 \exp\left(\frac{-Q_G}{RT}\right) \tag{6}$$

where R is the gas constant, T is absolute temperature, and Q_N and Q_G are the activation energies for nucleation and growth, respectively (Ranganathan & Von Heimendahl, 1981).

Under isothermal conditions, temperature, T, is independent of time and, thus, N and G can be treated as constants for the solution of the integrals in equation (4) (Avrami, 1940), giving

$$X(t) = 1 - \exp\left[-K(t - t_c)^{m+1}\right] \tag{7}$$

where $t - t_c$ is the time elapsed since the beginning of the transformation at the critical time, t_c, and K is a rate parameter (units: time^{-1}):

$$K = \frac{\alpha N G^m}{m+1} = \frac{\alpha N_0 {G_0}^m}{m+1} \exp\left(\frac{-Q_N + mQ_G}{RT}\right) \tag{8}$$

Equations (7) and (8) provide the solution for a particular case, in which nucleation occurs continuously through a transformation. Under some conditions, however, all nuclei are formed at the beginning of a transformation: a case known as site saturation (Cahn, 1956). Under site-saturated conditions, the nucleation rate can more appropriately be expressed as a product of the Dirac delta function, $\delta(t)$ (Woldt, 1992):

$$N = N_0 \exp\left(\frac{-Q_N}{RT}\right)\delta(t) \tag{9}$$

such that the solution of equation (4) provides

$$X(t) = 1 - \exp[-K(t - t_c)^m] \tag{10}$$

$$K = \alpha N G^m = \alpha N_0 {G_0}^m \exp\left(\frac{-Q_N + mQ_G}{RT}\right) \tag{11}$$

From the solutions provided in equations (7)–(11), a general form of the Avrami law is reached (Avrami, 1940; Farjas & Roura, 2006; Humphreys & Hatherly, 2004; Woldt, 1992):

$$X = 1 - \exp(-K(t - t_c)^n) \tag{12}$$

where the Avrami exponent, n, depends on the spatial and temporal dimensionality of growth and nucleation and is equal to $m + 1$ (i.e., $0 < n \leq 4$, representing transformation in up to three spatial dimensions, plus

one temporal dimension) for continuous nucleation (equation (7)) and equal to m (i.e., $0 < n \leq 3$, or transformation in up to three spatial dimensions, with no temporal dimensionality) under site-saturated conditions (equation (10)).

The Avrami rate parameter, K, may also be generalized as follows:

$$K = K_0 \exp\left(\frac{-Q_T}{RT}\right) \tag{13}$$

where Q_T represents an effective activation energy for the transformation and incorporates the activation energies of both nucleation and growth ($Q_T = Q_N + mQ_G$), while the pre-exponent, K_0, is given by $\alpha N G^m/(m+1)$ for continuous nucleation and $\alpha N G^m$ for site-saturated nucleation.

2.2. Modification for Dynamic Conditions

In the case of both static and dynamic recrystallization, transformation involves the nucleation of strain-free recrystallized grains, at the expense and consumption of highly-strained relict (original) grains (Figure 1), thereby lowering the total elastic strain energy (associated with free lattice defects) of the deformed material.

To describe the kinetics of DRX, we use a modified form of the generalized Avrami equation (equation (12)), following Shigematsu (1999) and Fernández et al. (2003), in which DRX is expressed as a function of strain, rather than time. We herein refer to this as the *dynamic* form of the Avrami equation, in that it applies to dynamic recrystallization:

$$X = 1 - \exp(-\beta(\gamma - \gamma_c)^n) \tag{14}$$

where $\gamma - \gamma_c$ is the strain accommodated since the onset of DRX at the critical strain, γ_c, and β (dimensionless) represents the rate of transformation, being functionally equivalent to K in equations (7)–(13):

$$\beta = \beta_0 \exp\left(\frac{-Q_{DRX}}{RT}\right) \tag{15}$$

The reasons for expressing DRX as a function of strain (rather than time) are threefold: (1) it enables us to directly compare DRX data from experiments conducted at different strain rates, (2) strain is often easier to quantify in a field setting, and (3) dislocation motion and therefore DRX are strain-dependent processes under deviatoric stress conditions.

Investigation of the Avrami kinetic parameters, β and n, may reveal important information regarding the kinetics and mechanisms of DRX. As stated above, the Avrami exponent, n, is known to depend on the spatial and temporal dimensionality of nucleation and growth, having a maximum value of 4, representing continuous nucleation through time with growth in three dimensions. Values of $n < 4$ are generally interpreted as a restriction in the kinetics of nucleation and/or growth (see Christian, 1965, pp. 546). For example, Cahn (1956) showed that n may decrease through a transformation if nucleation sites become exhausted (i.e., the site-saturation case), such that no further nucleation takes place.

During recrystallization, grain nucleation occurs by two primary mechanisms: *discontinuous* grain boundary bulging and *continuous* subgrain rotation (Platt & Behr, 2011; Sakai, 1989; Shimizu, 2008; Urai et al., 1986). Bulging nucleation primarily occurs along the boundaries between adjacent grains, and is driven by local differences in lattice strain energy, causing boundaries to migrate in the direction of the greatest defect density. Subgrain rotation nucleation, on the other hand, occurs under conditions where climb-assisted recovery is efficient, such that free dislocations can self-organize into subgrain walls, which progressively increase their rotational misorientation (as more dislocations of the same sign are added) until a high-angle grain boundary is formed.

In their theoretical treatment of DRX kinetics, Roberts et al. (1979) examined the effects of site saturation as a consequence of bulging recrystallization. They proposed that once nucleation sites along the boundaries of relict grains are exhausted, nucleation continues at a lesser rate along the boundaries of the primary recrystallization front, causing a decrease in n during DRX. If, however, nucleation occurs via subgrain rotation, where nuclei are not restricted to grain boundaries and can form within grains, site saturation is less likely to occur (Shigematsu, 1999), giving a constant value of n during DRX. We speculate, therefore, that

systematic variations in the Avrami kinetic parameters (particularly n) may reveal different DRX regimes with distinct nucleation mechanisms and/or growth kinetics (similar to those described by Hirth & Tullis, 1992, for instance).

3. Methods and Data

We have compiled and, in some cases, derived DRX data (i.e., recrystallized fraction measured at various strains; Table S1) from 12 published experimental studies on calcite (Barnhoorn et al., 2004; Pieri et al., 2001; Ter Heege et al., 2002; Valcke et al., 2015), quartz (Heilbronner & Tullis, 2006; Muto et al., 2011), olivine (Bystricky et al., 2000; Skemer et al., 2011) and ice (Vaughan et al., 2017), as well as austenitic steel (Fernández et al., 2003; Medina & Hernandez, 1996) and bischofite (Urai, 1987), which can be considered crystalline rock analog materials. Of all the experimental DRX data available for geologic materials, only the high temperature (~900 °C) calcite data of Ter Heege et al. (2002) and Valcke et al. (2015) were not included in the following analysis, as these authors observed only incipient (<20%) recrystallization. However, the 730 °C data from these studies were used to complement the 727 °C data of Pieri et al. (2001) and Barnhoorn et al. (2004). For comparison, all the available calcite data are provided in supporting information Figure S1.

While DRX data are available from some field studies (Pennacchioni et al., 2010; Shigematsu, 1999), we begin by examining only the data from laboratory experiments, for which the conditions of deformation (namely, temperature, pressure, stress, strain, and strain rate) are well constrained. Crucially, an assumption of isothermal (time-independent temperature) conditions is required for a straightforward solution of the integrals in equation (4); this assumption is reasonable under experimental conditions where (1) constant temperatures are imposed, (2) sample sizes are sufficiently small that shear heating is minimal, and (3) thermal gradients are sufficiently large that any heat produced by shearing is quickly dissipated. An extension of our analysis to nonisothermal conditions is beyond the scope of the present study but is briefly discussed below (section 5.4).

Recrystallized fractions, while determined using different techniques—electron backscatter diffraction (EBSD; Valcke et al., 2015; Vaughan et al., 2017), computer-integrated polarization (CIP) microscopy (Heilbronner & Tullis, 2006), and light optical micrograph analysis (Barnhoorn et al., 2004; Bystricky et al., 2000; Fernández et al., 2003; Medina & Hernandez, 1996; Muto et al., 2011; Pieri et al., 2001; Skemer et al., 2011; Ter Heege et al., 2002; Urai, 1987)—all represent the area fraction of material that has undergone recrystallization at a given strain, examined over two-dimensional sections in the plane containing the shear direction and shear plane normal (or, in axial compression experiments, prepared in a plane containing the shortening direction). We have not attempted to identify or incorporate any systematic errors that may be introduced by determining recrystallized fraction via different analytical techniques.

Recrystallized fraction measurements were not provided in the studies on olivine (Bystricky et al., 2000; Skemer et al., 2011) or ice (Vaughan et al., 2017) and have been determined here (supporting information Figures S2–S5) using the following methods.

3.1. Derivation of Olivine DRX Data

For olivine, recrystallized area fractions were measured by tracing regions of the published optical micrographs (supporting information Figure S2) containing small, subequant grains with low intragranular lattice distortions (i.e., uniform extinction) and often conspicuous parent-daughter grain relationships: common criteria for identifying recrystallized grains in geologic materials (Cross et al., 2017; Halfpenny et al., 2006; Platt & De Bresser, 2017; Valcke et al., 2015; Van der Wal et al., 1993). Regions of the optical images that were in extinction, or comprised of decompression cracks, were not included in the determination of recrystallized fraction.

3.2. Derivation of Ice DRX Data

The determination of recrystallized fraction for the ice data of Vaughan et al. (2017) was more complex than for other materials described in this study. Whereas the other materials analyzed here underwent net grain size reduction during DRX, the experimental ice samples of Vaughan et al. (2017), which were deformed close to their melting temperature ($T = -5$ °C; $T/T_m = 0.98$), exhibited bulk grain coarsening during deformation (supporting information Figure S4). This grain coarsening was attributed to the strain-energy-driven

consumption of grains poorly oriented for glide on the basal plane (i.e., low basal Schmid factors) by grains favorably oriented for glide on the basal plane (i.e., high basal Schmid factors; Vaughan et al., 2017), leading to the development of a small circle (i.e., cone) distribution of ice [c] axes around the compression axis (see also Qi et al., 2017). Here we determined the transformed (recrystallized) fraction of material using grain orientations measured by Vaughan et al. (2017) via EBSD. For a given strain, we calculated the area fraction of grains with basal Schmid factors ≥0.42 (following Vaughan et al., 2017), corresponding to grains with their basal planes inclined 45 ± 16° from the compression axis (see supporting information Figure S4). These values were then normalized to account for the area fraction of grains with high basal Schmid factors in the randomly oriented starting material (see supporting information Figure S5).

3.3. Derivation of the Critical Strain for DRX

The Avrami kinetic equations, given above, describe the progression of a transformation as a function of the time, t, elapsed since the onset of the transformation at the critical time, t_c. For the dynamic form of the generalized Avrami law used here (equation (14)), the transformation is instead expressed in terms of strain, $\gamma - \gamma_c$, where γ_c is the critical strain at which DRX begins. Numerous metallurgical studies have demonstrated that γ_c precedes the peak stress and onset of weakening in mechanical tests, leading to a relationship of the form:

$$\gamma_c = \varphi\gamma_p \tag{16}$$

where φ is the fraction of the peak strain, γ_p (i.e., the strain corresponding to the peak stress) at which the critical strain is found.

Physically, γ_c represents the point at which the amount of energy or work that can be locally stored in a crystal lattice is exceeded during loading (Wray, 1975) but may also be expressed as an energy dissipation rate threshold (Poliak & Jonas, 1996). In metallurgy, γ_c is often determined indirectly from experimental mechanical data (see Poliak & Jonas, 1996; Fernández et al., 2003, for details), with reported values for φ varying between 0.4 (Huang et al., 2007) and 0.95 (Medina & Hernandez, 1996). However, γ_c values determined indirectly via mechanical data do not necessarily represent the true onset of DRX; rather, these values give the strain at which the amount of DRX produces measurable softening (i.e., where stress or strain rate changes exceed the resolution of the deformation apparatus load cell or displacement transducer, respectively).

Here we determine γ_c directly through microstructural observation, defining it as the strain at which the recrystallized fraction, X, increases from zero to a nonzero value (Figure 2a); in other words, the strain at which the first recrystallized grain appears. In many cases, γ_c is well constrained within a narrow strain window. However, in some cases, γ_c is poorly constrained, for example, in quartz, where the first observation is given at $X = 45\%$, with no lower bound on γ_c (i.e., $X = 0\%$ at $\gamma > 0$).

We tested several methods for determining γ_c. Of these, only one method did not require us to impose an arbitrary or subjective lower bound on γ_c for the poorly constrained data. Here we perform a linear fit to the DRX data in γ-X space and extrapolate backward to find the x intercept, γ_c (Figure 2a). For each data set, the linear regression is performed only for the first two points with $X > 0$, although in cases where a lower bound on γ_c is available, we also include this point. Full details on the method are provided in supporting information Text S1.

By plotting our derived γ_c values versus peak strains determined, where possible, from the published mechanical data, we find that most of the points lie on a linear trend defined by $\gamma_c = 0.71\gamma_p$ (Figure 2b), consistent with the published metallurgical values ($0.4 \leq \varphi \leq 0.95$). It is worth pointing out here that the γ_c values for calcite DRX diverge from this relationship, such that γ_c increasingly exceeds γ_p as temperature decreases. We return to this point in the discussion.

4. Results

For each set of experiments, we fit the data using the dynamic form of the Avrami equation, according to the following derived directly from equation (14):

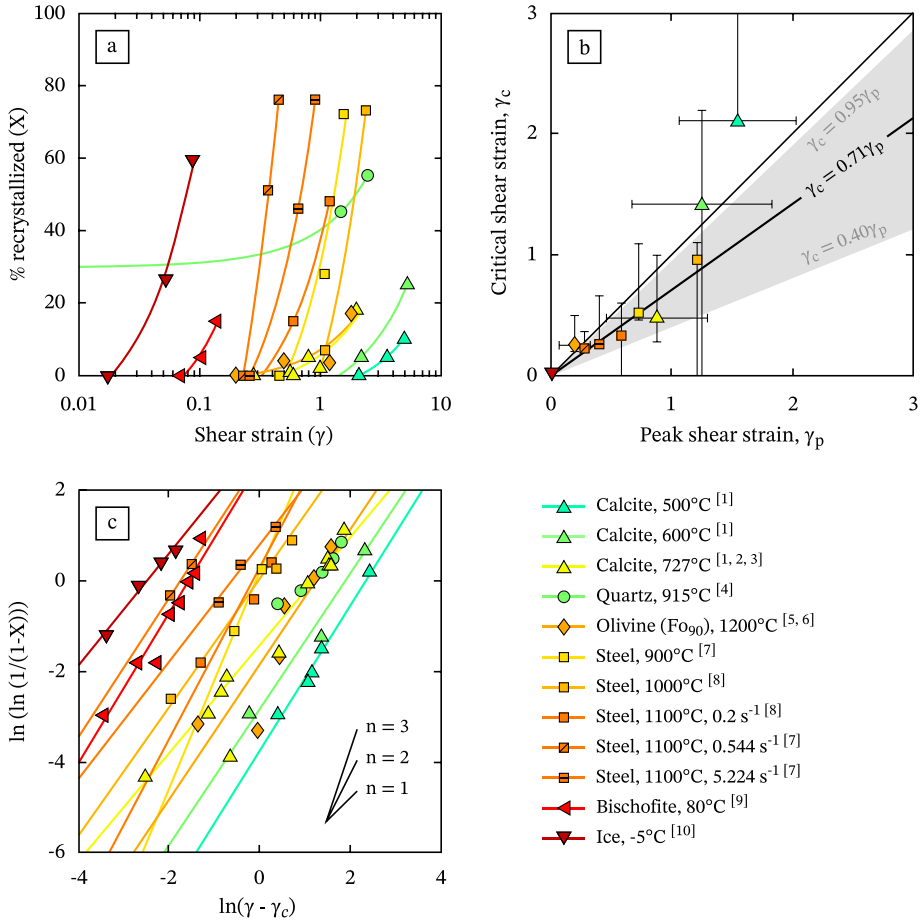

Figure 2. Derivation of (a and b) the critical strain, γ_c, and (c) the Avrami parameters β and n (equation (14)), used to construct the Avrami curves in Figure 3. (a) The critical strain, γ_c, at which DRX begins is found by linear regression of the DRX data in γ-X space (note that linear regression in log-linear space produces a curve), where the x intercept yields γ_c. (b) Most of these γ_c values fall within 40%–95% of the strain, γ_p, at which peak stress is observed (gray region). (c) Once γ_c is known, the Avrami parameters, β and n, can be obtained by linear regression of the data in $\ln(\gamma - \gamma_c)$ versus $\ln(-\ln(1-X))$ space (equation (17)). The data are from experiments on calcite ([1] = Barnhoorn et al., 2004; [2] = Pieri et al., 2001; [3] = Valcke et al., 2015), quartz ([4] =Heilbronner & Tullis, 2006), olivine ([5] = Bystricky et al., 2000; [6] = Skemer et al., 2011), austenitic steel ([7] = Medina & Hernandez, 1996; [8] = Fernández et al., 2003), bischofite ([9] = Urai, 1987), and ice ([10] = Vaughan et al., 2017).

$$\ln[-\ln(1-X)] = n\ \ln(\gamma-\gamma_c) + \ln(\beta) \tag{17}$$

where n and $\ln(\beta)$ are the slope and y intercept, respectively, of linear regressions through the data in $\ln(\gamma-\gamma_c)$ versus $\ln[-\ln(1-X)]$ space (Figure 2c). The derived values are provided in supporting information Table S2. Note that we did not fit the quartz data of Heilbronner and Tullis (2006), which do not follow a linear trend in Avrami space (Figure 2c) and for which we were unable to accurately determine γ_c (Figure 2a).

Figure 3 shows shear strain, γ, versus recrystallized fraction, X (0% to 100%) for the experimental data outlined above, with data points colored according to the homologous temperature (the fraction of a material's melting temperature, T/T_m) at which each experiment was performed. For the unconfined experiments on steel, bischofite, and ice, T_m was taken as the melting temperature at atmospheric pressure (P = 1 atm). For the confined experiments on calcite (P = 300 MPa) and quartz (P = 1,500 MPa), T_m was taken as 1350 °C (Suito et al., 2001) and 1990 °C (Jackson, 1976), respectively. For forsterite (Fo_{90}), we take T_m as 1770 °C, based on the melting temperature of Fo_{90} at P = 1 atm (Presnall, 1995). However, for Fo_{100}, T_m increases by 20 °C from P = 1 atm to P = 300 MPa (Presnall, 1995), such that T_m = 1770 °C may be a slight underestimation, translating to an error in T/T_m of ~0.01 (1%). We did not account for the influence of water content

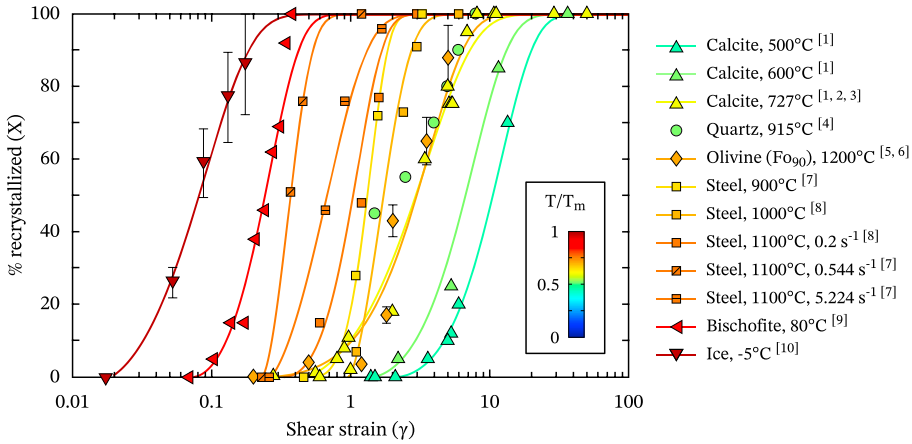

Figure 3. Dynamically recrystallized fraction, X, as a function of shear strain, γ. Errors of ±10% and ±16% in recrystallized fraction are given for the olivine and ice data, respectively, which were derived here (supporting information Figures S2–S5). The sigmoidal curves are fits to the data given by the Avrami equation (see Figure 2c). No Avrami curve is given for the quartz data of Heilbronner and Tullis (2006), which were poorly fit by the Avrami equation. The data and Avrami curves are colored according to the homologous temperature (fraction of each material's melting temperature, T/T_m) at which each set of experiments was conducted.

on melting temperatures. For reference, the experiments on calcite, olivine, and steel were all performed under nominally dry conditions.

For each experimental data set, recrystallized fraction increases monotonically with increasing strain (Figure 3), following a sigmoidal path in $\log_{10}(\gamma)$-X space that is delineated by the corresponding Avrami curve, derived using equation (17). The data show a strong thermal dependence, with DRX occurring over smaller strain magnitudes as homologous temperature increases. For example, calcite undergoes recrystallization over shear strains of 2–40 at a temperature (T = 500 °C; T/T_m = 0.48) close to that of the brittle-ductile transition (nominally T/T_m = 0.3). In contrast, ice fully recrystallizes within a shear strain of 0.5 at a temperature very close to its melting point (T = −5 °C; T/T_m = 0.98). To further demonstrate this thermal dependence, we plot the shear strain required to reach 1% ($\gamma_{0.01}$) and 99% ($\gamma_{0.99}$) recrystallization, as a function of homologous temperature (Figure 4), using values extracted from the curves shown in Figure 3. We find a strong ($R^2 > 0.9$) inverse relationship between homologous temperature and the shear strain required to reach a given amount of recrystallization, with 1% DRX occurring within shear strains of ~0.02–10

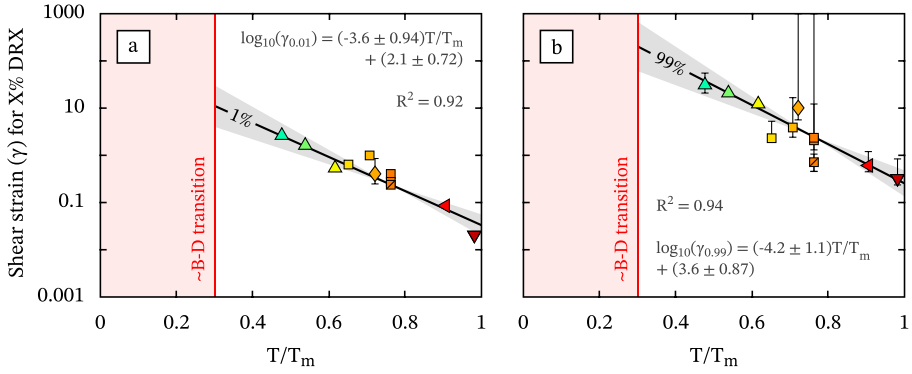

Figure 4. Homologous temperature, T/T_m, versus the shear strains, (a) $\gamma_{0.01}$ and (b) $\gamma_{0.99}$, required to reach 1% and 99% recrystallization, respectively, determined using the Avrami equation (equation (14)) and Avrami parameters derived in Figure 2c. The symbols are the same as those used in Figure 3. Equations for the linear regressions (black lines) are shown with 95% confidence intervals (gray shaded regions). The error bars represent the goodness-of-fit of the Avrami equation (equation (14)) to the data in Figure 2c. For reference, the nominal brittle-ductile (B-D) transition is shown at T/T_m = 0.3 (red line). DRX = dynamic recrystallization.

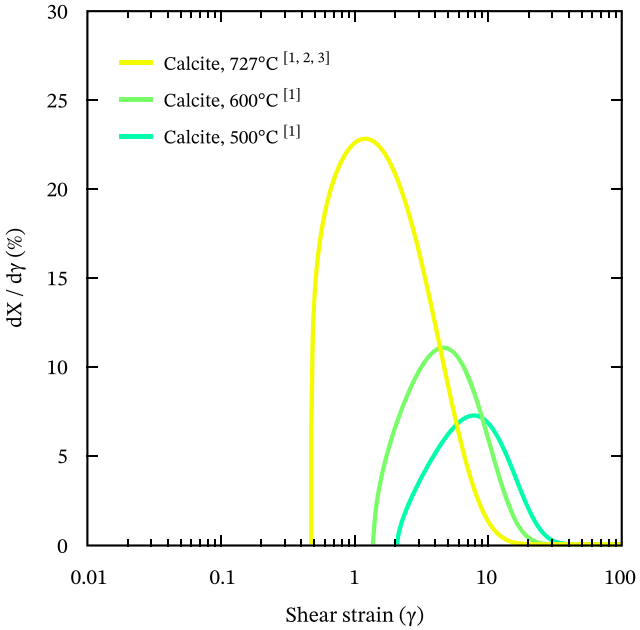

Figure 5. Dynamic recrystallization rate, $dX/d\gamma$, as a function of shear strain, γ, for calcite (data from [1] = Barnhoorn et al., 2004; [2] = Pieri et al., 2001; [3] = Valcke et al., 2015). Curves are calculated from the first derivative of the Avrami equation: $dX/d\gamma = n\beta(\gamma-\gamma_c)^{n-1}\exp(-\beta(\gamma-\gamma_c)^n)$. Note that the asymmetry of the curves arises from their truncation at the critical strain, γ_c (Figure 3).

(Figure 4a) and 99% DRX occurring within shear strains of 0.2–200 (Figure 4b), over the range of temperature conditions under which creep deformation typically occurs in nature (nominally $0.3 \leq T/T_m < 1$).

5. Discussion

5.1. Interpretation of Avrami Curves

The DRX data (Figure 3) follow sigmoidal paths in $\log_{10}(\gamma)$-X space that are typical of Avrami-type transformations, with lower rates of DRX near the start and end of the transformation, as shown by the first derivatives of the Avrami curves (Figure 5). Generally, the acceleration of recrystallization near the start of a transformation is interpreted as an incubation period relating to the accumulation of free dislocations, which provide the necessary driving force for grain nucleation (e.g., Stüwe et al., 2002). For example, grain boundary bulge nuclei will only form if the reduction in lattice strain energy (from sweeping out free lattice defects) is greater than the increase in grain boundary surface energy associated with creating a given bulge (Derby & Ashby, 1987; Platt & Behr, 2011).

As bulk dislocation density increases toward a steady state, DRX accelerates as more regions of the deforming material locally exceed the energetic threshold for nucleation (Derby & Ashby, 1987). The transformation continues to accelerate until eventually it reaches a maximum rate near 50% recrystallization, represented by a steepening of the Avrami curves (Figure 3) and a peak in the first derivative of the dynamic Avrami equation, $dX/d\gamma$ (Figure 5). Below, we show that the $dX/d\gamma$ curves peak at a strain closely corresponding to that of the point of maximum energy dissipation (see section 5.3.2).

Beyond the DRX rate peak, the transformation begins to decelerate toward completion (Figures 3 and 5). Under static conditions, this deceleration is commonly attributed to the impingement of growing nuclei against one another (Humphreys & Hatherly, 2004, pp. 232). However, recent studies on calcite (Platt & De Bresser, 2017) and quartz (Xia & Platt, 2018) have shown that during DRX, recrystallized grains have similar sizes to recrystallization nuclei (e.g., grain boundary bulges and subgrains). Such findings suggest that dynamically recrystallized grains do not grow significantly following nucleation, and grain growth therefore does not play a significant role during DRX (see also Roberts et al., 1979). Indeed, this inference is consistent with observations that in metals, DRX is *essentially a process of limited growth of the new recrystallized grains, with repeated nucleation* (Fernández et al., 2003), since DRX, unlike static recrystallization, involves the continuous generation of free dislocations (and associated elastic strain energy), which counteract grain coarsening driven by the minimization of grain boundary surface energy (Austin & Evans, 2007; De Bresser et al., 2001). One notable exception, however, occurs under high-temperature, grain boundary migration dominated conditions, where grains in favorable orientations grow at the expense of others (e.g., Qi et al., 2017; Vaughan et al., 2017; supporting information Figure S4) and DRX appears growth dominated, with limited nucleation. This exception aside, we infer that the slowing of DRX at large recrystallized fractions represents either (1) a reduction in the *volume* of unrecrystallized material available for grain nucleation or (2) a decrease in the *nucleation rate* in the unrecrystallized material. These two cases are subtly different and have distinct kinetics, which can be explored via the Avrami parameters, β and n.

5.2. Kinetics of DRX

5.2.1. Mechanisms of Recrystallized Grain Nucleation and Growth

The Avrami kinetic parameters, β and n (equations (14)–(15)), contain important information regarding the mechanisms of nucleation and growth. For example, the Avrami exponent, n, is commonly interpreted in terms of the spatial and temporal dimensionality of nucleation and growth (see Christian, 1965, pp. 546; Humphreys & Hatherly, 2004, pp. 234), being equal to a maximum value of 4 under conditions where nuclei form continuously and grow in three dimensions. Thus, changes in the Avrami parameters through a transformation may reveal changes in the dimensionality—and therefore the mechanisms—by which

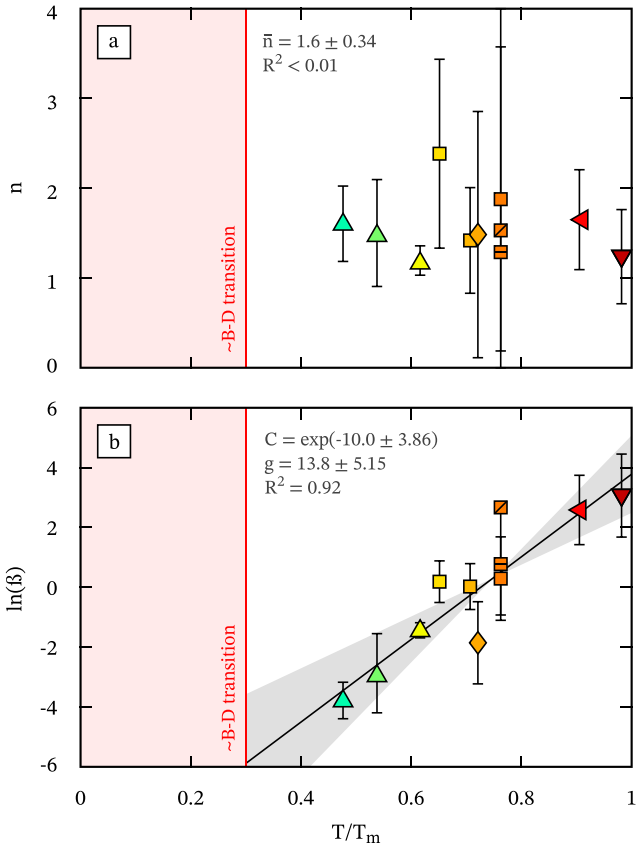

Figure 6. The Avrami parameters (a) n and (b) ln(β) as a function of homologous temperature, T/T_m. Symbols are the same as those used in Figure 3. The rate parameter ln(β) exhibits a strong correlation with T/T_m, which has been fit using linear regression (black line), with 95% confidence intervals represented by the gray shaded region. The error bars represent the goodness-of-fit of the Avrami equation (equation (14)) to the data in Figure 2c. For reference, the nominal brittle-ductile (B-D) transition is shown at $T/T_m = 0.3$ (red line).

nucleation and growth take place. For instance, previous theoretical treatments of transformation kinetics have shown that as a transformation progresses, nucleation sites may become exhausted, such that the rate of nucleation decreases (Cahn, 1956; Roberts et al., 1979). In this *site saturation* case, the temporal dependence of the Avrami exponent, n, will tend toward zero, giving a nonlinear trend to the data in Avrami space (e.g., Figure 2c). If site saturation is not achieved, the temporal contribution to n will remain constant, with $n \geq 1$.

With the exception of quartz (discussed later), each data set presented here is well described by a linear regression in Avrami space (see Figure 2c), implying constant (i.e., strain invariant) nucleation (and/or growth) rates through each transformation. In other words, nucleation site saturation is not achieved. This may reflect the activity of subgrain rotation nucleation, which is not confined to high-angle grain boundaries, thereby inhibiting site saturation (Shigematsu, 1999). Thus, we expect $n \geq 1$ for each data set and, specifically, $n \approx 1$, if we assume that growth plays a limited role during DRX. Indeed, all the experimental data have broadly consistent n values, with a mean value of 1.6 ± 0.34 (Figure 6a), indicating continuous nucleation with limited growth. For the most part, this finding is consistent with microstructural observations of the deformed samples, in which recrystallization nuclei have similar sizes to recrystallized grains. However, it is surprising to find that for ice, where DRX is growth dominated, n does not lie closer to 3: the value expected for three-dimensional growth with pre-existing nuclei. On the other hand, Christian (1965, pp. 546) states that n values of 1–1.5 can be representative of nuclei growing from an appreciable initial size; this is certainly the case for the ice samples analyzed here, which have an initial grain size of >300 μm (Vaughan et al., 2017). Alternatively, we speculate that n may also be relaxed if grain coarsening occurs by the coalescence of similarly oriented grains, rather than by normal grain growth. This process has been observed under comparably high-temperature, low-stress conditions in norcamphor (Herwegh et al., 1997) and quartz (Hongn & Hippertt, 2001).

Earlier, we speculated that systematic variations in the Avrami kinetic parameters, particularly n, would reveal different DRX regimes, similar to those reported by Hirth and Tullis (1992), where different nucleation and recovery mechanisms dominate under different thermomechanical conditions. However, we find similar n values (1.6 ± 0.34) across a broad range of homologous temperature ($0.5 \leq T/T_m < 1$). This finding does not necessarily mean that the primary nucleation mechanism (or relative activity of different nucleation mechanisms) is the same across this temperature range. Rather, this finding shows only that nucleation was continuous through each transformation (giving constant n, with $n \geq 1$). A change in n should only be expected where rotational nucleation is inhibited, such that all grain nucleation occurs by bulging confined to grain boundaries, leading to site saturation (e.g., Cahn, 1956; Roberts et al., 1979). Experiments at lower homologous temperatures ($T/T_m < 0.5$) may reveal such a transition.

5.2.2. Thermal Dependence of DRX Kinetics

While the Avrami kinetic parameters (β and n) appear constant (i.e., strain independent) within each experimental data set, we find that DRX kinetics are strongly dependent on temperature, whereby DRX both begins and reaches completion over an increasingly narrow range of shear strain with increasing homologous temperature, T/T_m (Figure 4). To further examine this thermal dependence, we plot β and n as a function of T/T_m (Figure 6).

As stated above, the Avrami exponents for each experiment are within error of one another ($n = 1.6 \pm 0.34$) and show no systematic variation with T/T_m ($R^2 \ll 0.1$; Figure 6a). The Avrami rate parameter, β (equations (14)–(15)), on the other hand, shows a strong positive correlation with T/T_m ($R^2 > 0.9$; Figure 6b),

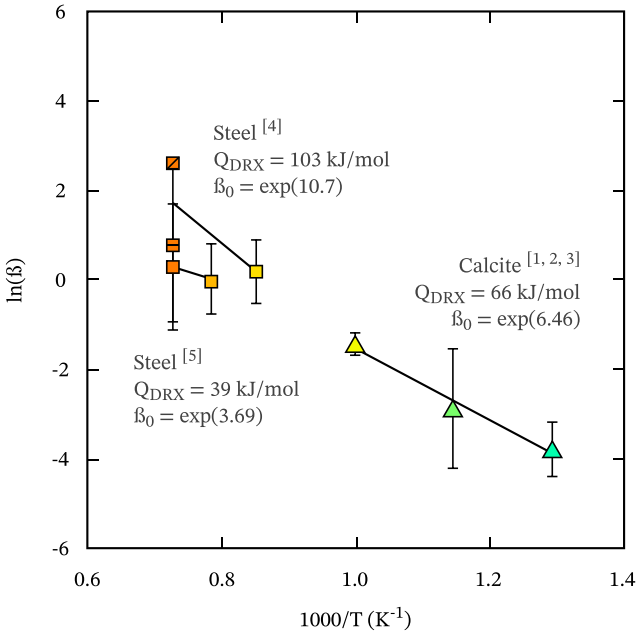

Figure 7. Arrhenius plots of 1,000/T versus ln(β), used to derive the activation energy for dynamic recrystallization, Q_{DRX} (equation (15)) for calcite ([1] = Barnhoorn et al., 2004; [2] = Pieri et al., 2001; [3] = Valcke et al., 2015) and steel ([4] = Medina & Hernandez, 1996; [5] = Fernández et al., 2003), which were studied at more than one temperature. Symbols are the same as those defined in Figure 3.

consistent with our observation that DRX rates increase as T/T_m increases (Figures 3–5). This dependence can be expressed in an Arrhenius-like form

$$\beta = C \exp\left(g\frac{T}{T_m}\right) \tag{18}$$

where C is analogous to the pre-exponential constant, β_0 (dimensionless) in equation (15), and g (also dimensionless) is a rate constant that prescribes exponentially increasing DRX rates with linearly increasing T/T_m. From linear regression through the data in Figure 6b, we obtain $C = \exp(-10.0 \pm 3.86)$ and $g = 13.8 \pm 5.15$. It is particularly interesting to highlight that the data—compiled from studies on a broad range of materials—can all be fit by a single solution to equation (18), suggesting an underlying material independence of DRX rates, at least to first order and as a function of homologous temperature.

Thermal dependence is widely observed in metals undergoing static recrystallization (e.g., Hutchinson et al., 1973) and is explicitly incorporated in the Avrami transformation model via Arrhenius functions describing the nucleation rate, N (equation (5)), and growth rate, G (equation (6)). From these equations, it is possible to individually obtain the activation energies for nucleation and growth (Q_N and Q_G, respectively), if N and G are known (Ranganathan & Von Heimendahl, 1981). However, N and G can be difficult to individually constrain, particularly in ex situ (i.e., time or strain series) experiments like those analyzed here. Instead, the activation energy of the transformation as a whole, Q_T (equation (13)), can be obtained from the Avrami rate parameter, K (β under dynamic conditions, in which case we refer to the activation energy for dynamic recrystallization, Q_{DRX}; equation (15)). As in rheological studies, the derivation of an activation energy may give insight into the rate-limiting process for DRX. Calculation of Q_{DRX} requires DRX data (i.e., recrystallized fraction as a function of strain) at more than one temperature for a given material. For many of the materials analyzed here, these data are not available. However, DRX data are available at more than one temperature in both calcite (Barnhoorn et al., 2004; Pieri et al., 2001; Valcke et al., 2015) and steel (Fernández et al., 2003; Medina & Hernandez, 1996); thus, we are able to estimate Q_{DRX} for these materials (Figure 7). For calcite, we obtain $Q_{DRX} = 66$ kJ/mol, while for steel we obtain $Q_{DRX} = 39$–103 kJ/mol. If we assume that growth plays a negligible role in DRX, Q_{DRX} gives the activation energy for nucleation, Q_N, since $Q_T = Q_N + mQ_G$ (equations (8)–(13)).

The value of Q_{DRX} (66 kJ/mol) found for calcite is significantly lower than that of both boundary (267 kJ/mol) and volume (382 kJ/mol) diffusion of calcium: the slowest diffusing species in calcite (Farver & Yund, 1996). Instead, Q_{DRX} falls closer to the activation energy for boundary diffusion of oxygen in calcite (127 kJ/mol; Farver & Yund, 1998). The boundary diffusivity of carbon in calcite is not known but, for both calcium and oxygen, the activation energy for boundary diffusion is lower than that of volume diffusion. Likewise, for steel, the derived values of Q_{DRX} (39–103 kJ/mol) fall closer to that of boundary diffusion in pure austenite (159 kJ/mol, compared to 270 kJ/mol for volume diffusion; Frost & Ashby, 1982), although the austenitic steels analyzed here contain multiple microalloying elements that may influence DRX kinetics. These findings are similar to those of Hutchinson and Ray (1979) who found that the activation energies for static recrystallization in copper fell below, but closer to, the activation energy for boundary diffusion. It has been suggested that the discrepancy between recrystallization and boundary diffusion activation energies may reflect an enhancement of atomic mobility provided by excess dislocations along the disordered boundaries of unrecrystallized grains (e.g., Wang et al., 1996).

5.3. Other Factors Influencing DRX Rates

5.3.1. Stress

Thus far, we have considered only the role of temperature in influencing DRX rates. The thermal conditions of deformation are certainly important, as they strongly influence the efficacy of elastic strain energy

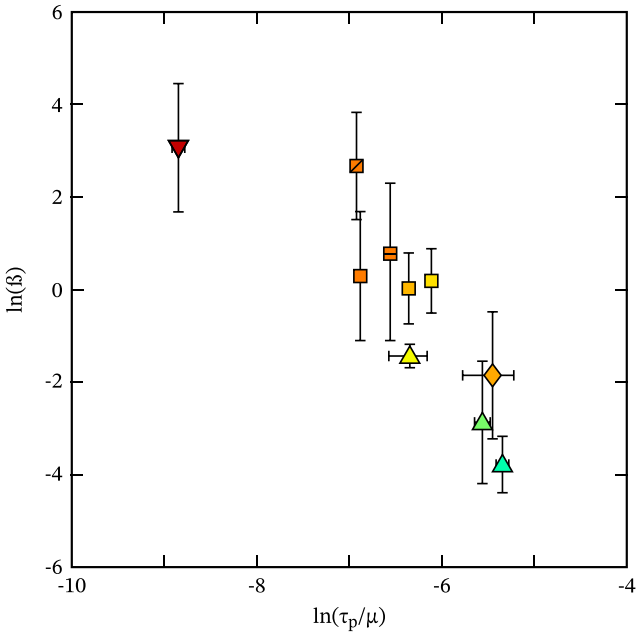

Figure 8. The Avrami rate parameter, β, as a function of peak shear stress, τ_p, normalized by shear modulus, μ, to enable comparison between different materials. Symbols are the same as those defined in Figure 3.

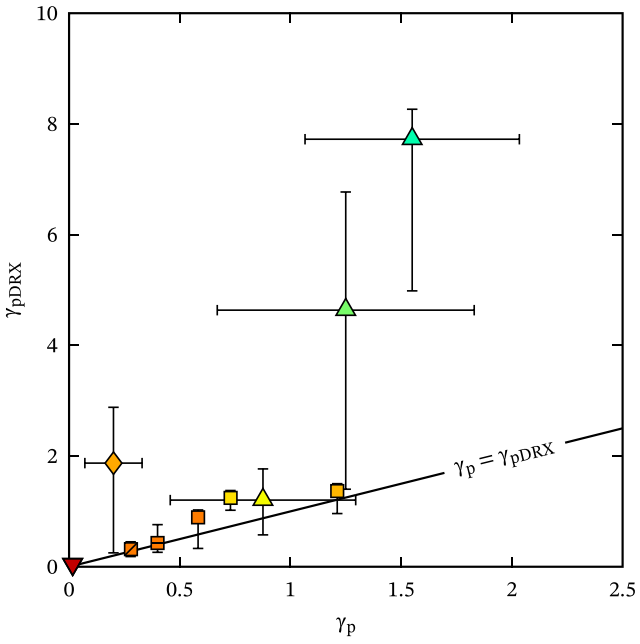

Figure 9. Mechanical peak strain, γ_p (i.e., the strain corresponding to the peak of the stress-strain curves), versus the dynamic recrystallization (DRX) peak strain, γ_{pDRX} (i.e., the strain corresponding to the peak of the DRX rate, dX/dγ curves shown in Figure 5). Most of the data fall, within error, on a 1:1 line (where $\gamma_p = \gamma_{pDRX}$). Symbols are the same as those used in Figure 3.

minimization through dislocation recovery and recrystallization, which rely on thermally activated diffusive processes (e.g., dislocation climb and vacancy diffusion). However, recovery and recrystallization are, ultimately, driven by the density of free dislocations, which roughly scales with the square of stress (Poirier, 1985, pp. 109). We must, therefore, consider the effects of both temperature *and* stress.

To investigate the influence of stress on DRX rates, we plot the Avrami rate parameter, β, as a function of the mean peak shear stress, τ_p, for each suite of experiments, normalized by the shear modulus, μ, of each material (Figure 8). We normalize by μ to enable comparison between the different materials, and use the peak stress, rather than the flow stress, as this is a more appropriate proxy for the driving force behind DRX. Whereas we find a positive correlation between T/T_m and β (Figure 6b), we find an inverse relationship between τ_p/μ and β (Figure 8). In other words, DRX is fastest under high-temperature, low-stress conditions. This is a seemingly counterintuitive result (and contradicts the recent findings of Holtzman et al., 2018), since stress scales with dislocation density, which provides the driving force for DRX. We suggest, however, that under high-stress, low-temperature conditions, large densities of dislocations with limited mobility accumulate, leading to dislocation entanglement that inhibits DRX. Further experiments performed at the same temperature and over a range of stress (or vice versa) may provide important insight into the competition between elastic energy accumulation (i.e., the stress-dependent DRX driving force) and dissipation (i.e., thermally dependent recovery and recrystallization rates).

5.3.2. Work Rate

Some authors have suggested that microstructural evolution rates are a function of the mechanical work rate per unit volume, $\dot{W} = \sigma\dot{\varepsilon}$ (where σ is differential stress and $\dot{\varepsilon}$ is strain rate), rather than differential stress alone (Austin & Evans, 2007, 2009; Bercovici & Ricard, 2005; Poliak & Jonas, 1996; Rozel et al., 2011). In these models, mechanical work is dissipated as energy stored in dislocations and grain boundaries, plus heat production and other irreversible increases in entropy (e.g., Austin & Evans, 2007, 2009). Thus, grain boundary creation (i.e., DRX) is a dissipative response to mechanical work, and we must also, therefore, investigate the relationship between $\dot{W}$ and DRX rates, the latter being represented by β.

In contrast to temperature and stress, which are strongly correlated with DRX rate (Figures 6b and 8, respectively), we find no strong relationship between the mean peak work rate ($\tau_p\dot{\gamma}$, where $\dot{\gamma}$ is shear strain rate) and β (supporting information Figure S6a). Normalizing the data to a constant value of T/T_m using equation (18) likewise produces no strong relationship (supporting information Figure S6b). However, we find a near 1-to-1 correlation between the mechanical peak shear strain, γ_p (equation (16)), and the DRX peak shear strain, γ_{pDRX} (Figure 9), the latter being the strain corresponding to the peak of the DRX rate (dX/dγ) curves (Figure 5). In other words, DRX rates and, therefore, energy dissipation rates (due to DRX) are fastest at the point of maximum deformation work rate. A notable exception is found for calcite, which increasingly diverges from this 1:1 relationship as temperature decreases (Figure 9), such that at lower temperatures, DRX lags behind the application of mechanical work. Earlier, we also noted that the critical strains, γ_c, for the onset of calcite DRX increasingly exceed the peak strains, γ_p, as temperature decreases

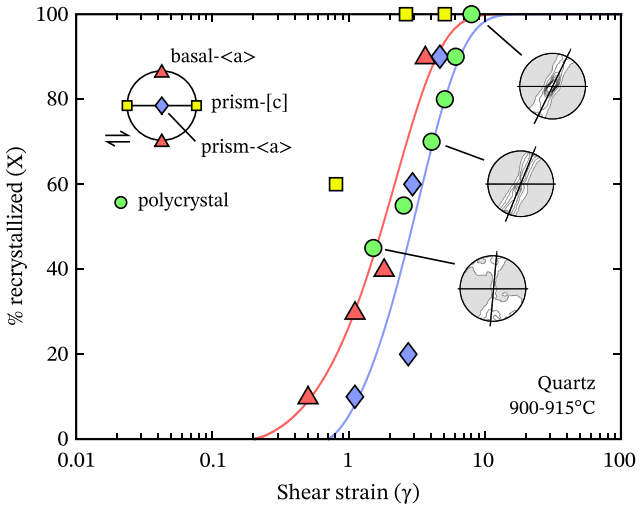

Figure 10. Dynamically recrystallized fraction as a function of shear strain for experiments on quartz single crystals (Muto et al., 2011) and polycrystals (Heilbronner & Tullis, 2006). All experiments were performed at 900–915 °C and 1.5 GPa confining pressure. Quartz c[0001] axis pole figures (modified after Heilbronner & Tullis, 2006) are shown for the polycrystalline samples deformed to shear strains of 1.5, 4, and 8, to highlight an observed transition from basal-<*a*> to prism-<*a*> dominated glide.

(Figure 2b). Together, these findings suggest that DRX is delayed at low temperatures in calcite. Given that weakening cannot occur without the dissipation of internal strain energy, other dissipative processes must dominate at low strains, before the onset of DRX. We interpret this process to be deformation twinning, which becomes increasingly pervasive as temperature decreases (compare Figures 3–5 in Barnhoorn et al., 2004). Put simply, DRX occurs over longer strain scales where other dissipative processes are in operation.

5.3.3. Crystal Orientation

While most of the compiled DRX data are fit well by the Avrami model (equation (14)), the quartz DRX data of Heilbronner and Tullis (2006) do not follow a linear trend in Avrami space (Figure 2c) and, as a result, are poorly fit by the Avrami equation. Assuming that this irregular trend is not the result of measuring error, the data suggest that DRX in quartz accelerates after ~40% recrystallization. A similar observation in plagioclase from the Hatagawa shear zone (Shigematsu, 1999) was attributed to two-stage recrystallization, following the model of Roberts et al. (1979). In the Roberts et al. model, recrystallized grain nucleation initially occurs along the boundaries of original grains and decelerates as these primary nucleation sites become exhausted (i.e., site saturated), with $dX/d\gamma$ approaching zero (see, for example, Figure 1c in Shigematsu, 1999). Recrystallization continues once a sufficient driving force is established to initiate a secondary stage of nucleation along the boundaries of the recrystallization front. For the quartz data of Heilbronner and Tullis (2006), the acceleration of DRX beyond $X = 40\%$ would represent this second stage of nucleation and DRX. However, it is not clear if this model is appropriate for these samples, which display fine-grained microstructures very similar to those of the other materials studied here. To further examine the rates of DRX in quartz, we compare DRX data for quartz polycrystals (Heilbronner & Tullis, 2006) and oriented single crystals (Muto et al., 2011) in Figure 10. Crucially, these two experimental studies were performed under nominally the same conditions (T = 900–915 °C; P = 1.5 GPa; $\dot{\gamma} = 1 \times 10^{-5}$–$4 \times 10^{-5}$ s^{-1}; water content = 200–700 ppm H/Si).

The single crystal data show DRX rates that vary by up to an order of magnitude. Single crystals oriented for glide on the stronger prism-[*c*] slip system undergo recrystallization most rapidly (critical shear strains for 90% recrystallization, $\gamma_{0.90} \approx 1$), while single crystals oriented for glide on the weaker basal-<*a*> and prism-<*a*> slip systems recrystallize more slowly ($\gamma_{0.90} \approx 4$ and $\gamma_{0.90} \approx 6$, respectively). Meanwhile, the DRX data for the polycrystalline samples initially fall on the Avrami curve for basal-<*a*> single crystals but, at a shear strain of between 1.5 and 4, transition onto the Avrami curve for prism-<*a*> single crystals (Figure 10). Notably, this transition coincides with a switch from a basal-<*a*> dominated crystallographic preferred orientation (CPO), to a prism-<*a*> dominated CPO in the polycrystalline samples (Heilbronner & Tullis, 2006). Put simply, the data suggest a change in DRX kinetics as CPO evolves and different slip systems become dominant. This observation is particularly interesting given the recent finding of (at least) two dislocation creep regimes for quartz—one dominated by basal-<*a*> fabrics and the other by prism-<*a*> fabrics—depending on the rate-limiting deformation process (Tokle et al., 2019).

In metals, it has long been observed that grains in certain orientations can accommodate large plastic strains with minimal recrystallization, while grains in other orientations undergo rapid recrystallization (e.g., Somerday & Humphreys, 2003). Likewise, natural vein quartz from the Italian Alps has been shown to recrystallized heterogeneously, depending on crystal orientation, with quartz veins in prism-<*a*> orientations undergoing complete recrystallization between shear strains of 3 and 4, and quartz veins in harder, prism-[*c*] orientations accommodating no appreciable deformation or recrystallization (Pennacchioni et al., 2010). Note that this differs from the experimental observations, where prism-[*c*] oriented crystals undergo the most rapid DRX, perhaps because no softer slip systems are available for glide.

5.3.4. Initial Grain Size

Many authors have demonstrated the importance of grain size in controlling nucleation site availability and, therefore, DRX rate (e.g., El Wahabi et al., 2005; Fernández et al., 2003; Hutchinson et al., 1989; Jonas et al.,

2009; Roberts et al., 1979). In coarse-grained samples, the total area of grain boundaries per unit volume is less than in fine-grained samples and, thus, there are fewer sites available for nucleation by grain boundary bulging mechanisms. Previous studies on both engineering (e.g., Hutchinson et al., 1989; Roberts et al., 1979) and geologic (Shigematsu, 1999) materials have shown nucleation rates to decrease during recrystallization, particularly in coarse-grained samples (Hutchinson et al., 1989). In these studies, decreasing DRX rates were attributed to the saturation of nucleation sites, thereby lowering nucleation rates and causing a decrease in the Avrami exponent, n, as a function of time or strain. The DRX data analyzed here, however, show no appreciable change in n as a function of strain, and all (with the exception of quartz) are satisfactorily fit by a linear regression in Avrami space (Figure 2c). Furthermore, although most of the data examined here are given for a single starting grain size, we find no significant difference in DRX rate between olivine samples with vastly different starting grain sizes (15–32 μm, Bystricky et al., 2000, and 510 μm, Skemer et al., 2011)—see supporting information Figure S3. These results suggest that for the data analyzed here, DRX rates are largely insensitive to grain boundary area and the availability of grain boundary nucleation sites, perhaps implying a contribution from rotational nucleation, which, as other authors have noted, is not confined to grain boundaries and will not lead to site saturation (Shigematsu, 1999). Indeed, the influence of initial grain size on DRX rate is generally considered to become more pronounced at lower temperatures, under conditions where bulge nucleation dominates (e.g., El Wahabi et al., 2005). A component of subgrain rotation nucleation is also consistent with our interpretation of continuous nucleation at a fixed rate (constant n) and has been identified in many of the experimental samples analyzed here. Again, an interesting focus for future study would be to conduct experiments at low T/T_m (or high stress) conditions, to see if the Avrami kinetic parameters evolve through the transition from bulge- to rotation-dominated nucleation.

5.4. An Apparent, Material-Independent Law for DRX Rates

By incorporating our values of β (Figure 6b and equation (18)) and n (Figure 6a) into the modified Avrami law (equation (14)), we are able to calculate recrystallized fraction, X, as a function of both shear strain, γ, and homologous temperature, T/T_m:

$$X = 1 - \exp\left(-C\ \exp\left(g\frac{T}{T_m}\right)\ (\gamma - \gamma_c)^n\right) \tag{19}$$

where C, g, and n are all constants outlined above, such that the only variables are homologous temperature and strain. To reiterate, $C = \exp(-10.0 \pm 3.86)$, $g = 13.8 \pm 5.15$, and $n = 1.6 \pm 0.34$ (Figure 6). The surface defined by equation (19) satisfies, within error, all the DRX data compiled here, with the exception of the quartz data of (Heilbronner & Tullis, 2006), suggesting an underlying material independence of DRX rates, at least to first order.

This single fit to the experimental data is, potentially, a powerful tool for use as either a geothermometer (where shear strain and recrystallized fraction are known) or a strain meter (when temperature and recrystallized fraction are known). Moreover, by making some assumptions about the size and shape of recrystallized grains, it should be possible to (1) derive an expression for the rate of grain size reduction, based on the first derivative of equation (19), and (2) predict complete grain size distributions during DRX, for incorporation into rheological models of parallel dislocation and diffusion creep (e.g., Herwegh et al., 2005).

Strictly speaking, equation (19) is applicable only under isothermal conditions, where the rates of nucleation and growth are time independent (see equations (5) and (6)). As stated above, this assumption is sensible under experimental conditions where isothermal conditions are imposed, and any thermal perturbations due to shear heating are quickly dissipated. Natural shear zones, however, may experience complex thermal histories—during exhumation or subduction, for example—and are likely closer to adiabatic conditions such that shear heating may be significant (e.g., Foley, 2018; Holtzman et al., 2018). An extension of our analysis to nonisothermal conditions is beyond the scope of the present study. With that being said, we speculate that under conditions where microstructural evolution can keep pace with evolving temperatures, our findings (i.e., equation (19)) may still be applicable via a quasi-static approximation (similar to that employed by Holtzman et al. (2018) for the application of steady state flow laws to transient creep). Nevertheless, further experiments are required to test this approximation.

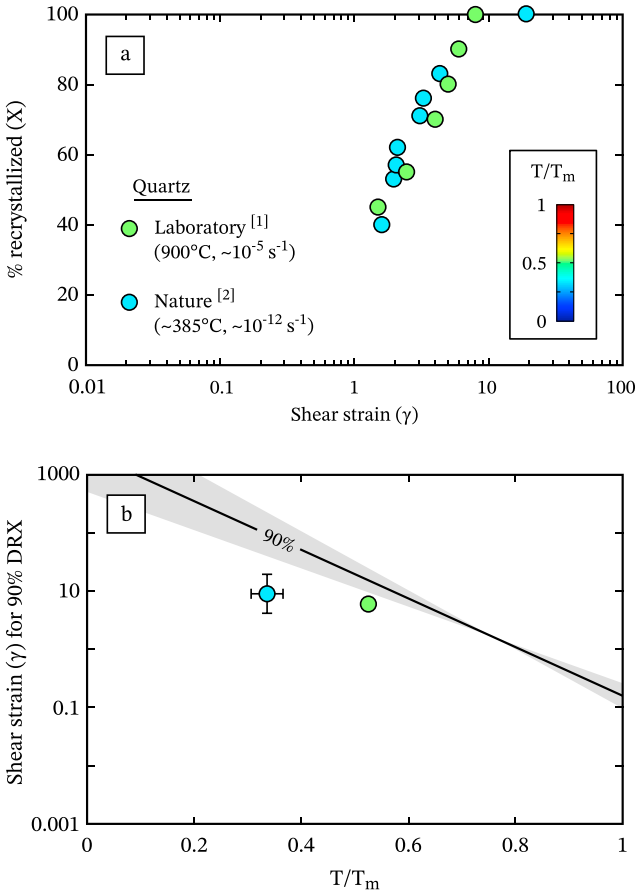

Figure 11. A comparison of dynamic recrystallization (DRX) rates in experimentally (green points; [1] = Heilbronner & Tullis, 2006) and naturally (blue points; [2] = Shigematsu, 1999) deformed quartz. (a) Dynamically recrystallized fraction versus shear strain. Points are colored according to the homologous temperature at which deformation occurred. (b) The shear strain required for 90% recrystallization, as a function of homologous temperature, T/T_m.

5.5. Extrapolation to Natural Conditions

The DRX data compiled in this study are fit well by equation (19), which incorporates a rate term that is sensitive to the homologous temperature of deformation. However, it remains to be seen whether this relationship is valid under natural (low temperature, stress, and work rate) conditions. Shigematsu (1999) provides the most complete analysis, to date, of DRX kinetics under natural geologic conditions, based on recrystallized fraction measurements in deformed granitoids from the Hatagawa shear zone, NE Japan. Here we compare the DRX rates of naturally (Shigematsu, 1999) and experimentally (Heilbronner & Tullis, 2006) deformed quartz (Figure 11), both of which predominately recrystallized by subgrain rotation nucleation.

The natural and experimental data show remarkably similar DRX rates (Figure 11a), despite significant differences in the conditions of deformation, including, notably, temperature. Whereas the quartz deformation experiments of Heilbronner and Tullis (2006) were performed at 900 °C, Shigematsu and Tanaka (2000) estimate deformation temperatures of 330–350 °C, using two-feldspar geothermometry (Stormer, 1975), for the shear zone studied by Shigematsu (1999). Consequently, the natural samples recrystallize faster than predicted from the experimental data (Figure 11b). However, deformation temperatures of 330–350 °C are lower than typically expected for quartz deforming within the subgrain rotation (SGR) regime, as defined by Stipp et al. (2002), which is constrained to lie within a temperature range of 400–500 °C under typical shear zone strain rates of 10^{-12} s^{-1}. Indeed, Shigematsu et al. (2009) reanalyzed deformation temperatures for the Hatagawa shear zone using the revised two-feldspar geothermometer of Whitney and Stormer (1977) and reported temperatures 40–90 °C higher than previously estimated. The maximum temperature range for the shear zone analyzed by Shigematsu (1999) is therefore 330–440 °C. Given that Na-K exchange between orthoclase and plagioclase can occur during cooling (i.e., after equilibration at syndeformation temperatures), it is likely that the shear zone described by Shigematsu (1999) deformed at temperatures near the upper end of this range, in consistency with the temperatures suggested for quartz SGR deformation (Stipp et al., 2002). Still, there remains a difference in T/T_m of ~0.2 (20%), between the experimental and natural samples (assuming T_m = 1685 °C at 300-MPa confining pressure; Jackson, 1976) and even these higher, revised temperatures are incapable of reconciling the discrepancy in DRX rates: the natural sample recrystallizes over a strain scale that is roughly an order of magnitude lower than that predicted by the experimental data (Figure 11b). Clearly, further study of DRX in natural settings is required for the reliable extrapolation of experimental DRX rates to natural conditions.

6. Summary and Closing Remarks

We have compiled and analyzed the rates of dynamic recrystallization (DRX) in geologic materials, using the Johnson-Mehl-Avrami-Kolmogorov (or Avrami) model for transformation kinetics. The DRX data were obtained from 12 published experimental studies on a wide range of geologic and engineering materials. We find the following:

1. DRX rates in laboratory experiments are strongly dependent on the homologous temperature of deformation and can be described by a single fit to a modified form of the Avrami equation (equation (19)), suggesting an underlying degree of material independence regarding DRX rates.
2. Under experimental conditions, DRX reaches completion within a shear strain of 0.2 near a material's melting temperature, and 200 at temperatures typical of the brittle-ductile transition, spanning 3

orders of magnitude. Thus, lithospheric rocks may evolve over long transient intervals, during which microstructure and rheology are not at steady state.

3. Activation energies for DRX have been determined at 39–103 kJ/mol and suggest that DRX is rate-limited by grain boundary diffusion.
4. The onset of DRX is delayed if other dissipative microstructural processes (e.g., deformation twinning) operate at low strains. The peak of experimental creep (e.g., stress-strain, or rate-strain) curves represents the point of maximum energy dissipation due to microstructural evolution.
5. Quartz DRX rates evolve in response to a transition from basal-<*a*> to prism-<*a*> dominated glide at intermediate strains.
6. The experimental data do not show a systematic dependence of DRX on deformation work rate (i.e., the product of stress and strain rate), which may reflect the limited range of strain rates tested in experimental studies. Indeed, natural DRX rates from the Hatagawa shear zone cannot be explained by variations in temperature alone.

To the best of our knowledge, this study provides the most complete analysis, to date, of DRX kinetics in geologic materials. Nevertheless, further work is required to explore the influence of different nucleation mechanisms, mechanical work rates, initial grain sizes, water contents, secondary phases, and other dissipative microstructural processes (e.g., deformation twinning) on DRX rates. This contribution provides a framework and motivation for future studies, with the ultimate goal of empirically constraining grain size evolution rates, due to DRX, in the Earth's interior.

Acknowledgments
This study was funded through an National Science Foundation grant (EAR-1352306) awarded to P. S. and support from the McDonnell Center for the Space Sciences for A. J. C. The data used in this study are available in Table S1 in the supporting information. We are grateful to M. Vaughan and D. Prior for providing their ice EBSD data and to all those whose published data we used here. Discussions with J. Wheeler regarding Avrami kinetics were extremely helpful, while detailed reviews by N. Shigematsu and B. Holtzman greatly improved both the content and clarity of this paper.

References

Austin, N., & Evans, B. (2009). The kinetics of microstructural evolution during deformation of calcite. *Journal of Geophysical Research*, *114*, B09402. https://doi.org/10.1029/2008JB006138

Austin, N. J., & Evans, B. (2007). Paleowattmeters: A scaling relation for dynamically recrystallized grain size. *Geology*, *35*(4), 343. https://doi.org/10.1130/G23244A.1

Avrami, M. (1940). Kinetics of phase change. II transformation-time relations for random distribution of nuclei. *The Journal of Chemical Physics*, *8*(2), 212–224. https://doi.org/10.1063/1.1750631

Barnhoorn, A., Bystricky, M., Burlini, L., & Kunze, K. (2004). The role of recrystallisation on the deformation behaviour of calcite rocks: Large strain torsion experiments on Carrara marble. *Journal of Structural Geology*, *26*(5), 885–903. https://doi.org/10.1016/j.jsg.2003.11.024

Barr, A. C., & McKinnon, W. B. (2007). Convection in ice I shells and mantles with self-consistent grain size. *Journal of Geophysical Research*, *112*, E02012. https://doi.org/10.1029/2006JE002781

Bercovici, D., & Ricard, Y. (2005). Tectonic plate generation and two-phase damage: Void growth versus grain size reduction. *Journal of Geophysical Research*, *110*, B03401. https://doi.org/10.1029/2004JB003181

Bercovici, D., & Ricard, Y. (2012). Mechanisms for the generation of plate tectonics by two-phase grain-damage and pinning. *Physics of the Earth and Planetary Interiors*, *202-203*, 27–55. https://doi.org/10.1016/j.pepi.2012.05.003

Braun, J., Chéry, J., Poliakov, A., Mainprice, D., Vauchez, A., Tomassi, A., & Daignières, M. (1999). A simple parameterization of strain localization in the ductile regime due to grain size reduction: A case study for olivine. *Journal of Geophysical Research*, *104*(B11), 25,167–25,181. https://doi.org/10.1029/1999JB900214

Bystricky, M., Kunze, K., Burlini, L., & Burg, J.-P. (2000). High shear strain of olivine aggregates: Rheological and seismic consequences. *Science (80-.)*, *290*(5496), 1564–1567. https://doi.org/10.1126/science.290.5496.1564

Cahn, J. W. (1956). The kinetics of grain boundary nucleated reactions. *Acta Metallurgica*, *4*(5), 449–459. https://doi.org/10.1016/0001-6160(56)90041-4

Carlson, W. D. (1983). Aragonite-calcite nucleation kinetics: An application and extension of Avrami transformation theory. *Journal of Geology*, *91*(1), 57–71. https://doi.org/10.1086/628744

Christian, I. J. W. (1965). *The Theory of Transformations in Metals and Alloys*. Oxford: Pergamon Press.

Covey-Crump, S. J. (1997). The normal grain growth behaviour of nominally pure calcitic aggregates. *Contributions to Mineralogy and Petrology*, *129*(2–3), 239–254. https://doi.org/10.1007/s004100050335

Cross, A. J., Ellis, S., & Prior, D. J. (2015). A phenomenological numerical approach for investigating grain size evolution in ductiley deforming rocks. *Journal of Structural Geology*, *76*, 22–34. https://doi.org/10.1016/j.jsg.2015.04.001

Cross, A. J., Prior, D. J., Stipp, M., & Kidder, S. (2017). The recrystallized grain size piezometer for quartz: An EBSD-based calibration. *Geophysical Research Letters*, *44*, 6667–6674. https://doi.org/10.1002/2017GL073836

Dannberg, J., Eilon, Z., Faul, U., Gassmöller, R., Moulik, P., & Myhill, R. (2017). The importance of grain size to mantle dynamics and seismological observations. *Geochemistry, Geophysics, Geosystems*, *18*, 3034–3061. https://doi.org/10.1002/2017GC006944

De Bresser, J. H. P., Ter Heege, J. H., & Spiers, C. J. (2001). Grain size reduction by dynamic recrystallization: Can it result in major rheological weakening? *International Journal of Earth Sciences*, *90*(1), 28–45. https://doi.org/10.1007/s005310000149

Derby, B., & Ashby, M. F. (1987). On dynamic recrystallisation. *Scripta Metallurgica*, *21*(6), 879–884. https://doi.org/10.1016/0036-9748(87)90341-3

El Wahabi, M., Gavard, L., Montheillet, F., Cabrera, J., & Prado, J. (2005). Effect of initial grain size on dynamic recrystallization in high purity austenitic stainless steels. *Acta Materialia*, *53*(17), 4605–4612. https://doi.org/10.1016/j.actamat.2005.06.020

Etheridge, M. A., & Wilkie, J. C. (1979). Grainsize reduction, grain boundary sliding and the flow strength of mylonites. *Tectonophysics*, *58*(1-2), 159–178. https://doi.org/10.1016/0040-1951(79)90327-5

Evans, B., Renner, J., & Hirth, G. (2001). A few remarks on the kinetics of static grain growth in rocks. *International Journal of Earth Sciences*, *90*(1), 88–103. https://doi.org/10.1007/s005310000150

Farjas, J., & Roura, P. (2006). Modification of the Kolmogorov-Johnson-Mehl-Avrami rate equation for non-isothermal experiments and its analytical solution. *Acta Materialia*, *54*(20), 5573–5579. https://doi.org/10.1016/j.actamat.2006.07.037

Farver, J. R., & Yund, R. A. (1996). Volume and grain boundary diffusion of calcium in natural and hot-pressed calcite aggregates. *Contributions to Mineralogy and Petrology*, *123*(1), 77–91. https://doi.org/10.1007/s004100050144

Farver, J. R., & Yund, R. A. (1998). Oxygen grain boundary diffusion in natural and hot-pressed calcite aggregates. *Earth and Planetary Science Letters*, *161*(1–4), 189–200. https://doi.org/10.1016/S0012-821X(98)00150-2

Faul, U. H., & Scott, D. (2006). Grain growth in partially molten olivine aggregates. *Contributions to Mineralogy and Petrology*, *151*(1), 101–111. https://doi.org/10.1007/s00410-005-0048-1

Fernández, A. I., Uranga, P., López, B., & Rodriguez-Ibabe, J. M. (2003). Dynamic recrystallization behavior covering a wide austenite grain size range in Nb and Nb-Ti microalloyed steels. *Materials Science and Engineering A*, *361*(1–2), 367–376. https://doi.org/10.1016/S0921-5093(03)00562-8

Foley, B. J. (2018). On the dynamics of coupled grain size evolution and shear heating in lithospheric shear zones. *Physics of the Earth and Planetary Interiors*, *283*, 7–25. https://doi.org/10.1016/J.PEPI.2018.07.008

Frost, H. J., & Ashby, M. F. (1982). *Deformation mechanism maps: The plasticity and creep of metals and ceramics*. Oxford: Pergamon Press.

Halfpenny, A., Prior, D. J., & Wheeler, J. (2006). Analysis of dynamic recrystallization and nucleation in a quartzite mylonite. *Tectonophysics*, *427*(1-4), 3–14. https://doi.org/10.1016/j.tecto.2006.05.016

Hall, C. E., & Parmentier, E. M. (2003). Influence of grain size evolution on convective instability. *Geochemistry, Geophysics, Geosystems*, *4*(3), 1029. https://doi.org/10.1029/2002GC000308

Heilbronner, R., & Tullis, J. (2006). Evolution of c axis pole figures and grain size during dynamic recrystallization: Results from experimentally sheared quartzite. *Journal of Geophysical Research*, *111*, B10202. https://doi.org/10.1029/2005JB004194

Herwegh, M., de Bresser, J. H. P., & ter Heege, J. H. (2005). Combining natural microstructures with composite flow laws: An improved approach for the extrapolation of lab data to nature. *Journal of Structural Geology*, *27*(3), 503–521. https://doi.org/10.1016/j.jsg.2004.10.010

Herwegh, M., Handy, M. R., & Heilbronner, R. (1997). Temperature- and strain-rate-dependent microfabric evolution in monomineralic mylonite: Evidence from in situ deformation of norcamphor. *Tectonophysics*, *280*(1–2), 83–106. https://doi.org/10.1016/S0040-1951(97)00139-X

Hiraga, T., Chihiro, T., Ohashi, N., & Sano, S. (2010). Grain growth systematics for forsterite ± enstatite aggregates: Effect of lithology on grain size in the upper mantle. *Earth and Planetary Science Letters*, *291*(1–4), 10–20. https://doi.org/10.1016/J.EPSL.2009.12.026

Hirth, G., & Tullis, J. (1992). Dislocation creep regimes in quartz aggregates. *Journal of Structural Geology*, *14*(2), 145–159. https://doi.org/10.1016/0191-8141(92)90053-Y

Holtzman, B. K., Chrysochoos, A., & Daridon, L. (2018). A thermomechanical framework for analysis of microstructural evolution: Application to olivine rocks at high temperature. *Journal of Geophysical Research: Solid Earth*, *123*, 8474–8507. https://doi.org/10.1029/2018JB015613

Hongn, F., & Hippertt, J. (2001). Quartz crystallographic and morphologic fabrics during folding/transposition in mylonites. *Journal of Structural Geology*, *23*(1), 81–92. https://doi.org/10.1016/S0191-8141(00)00051-1

Huang, G., Liu, Q., Wang, L., & Yin, X. (2007). Dynamic recrystallization of 3104 aluminum alloy during isothermal compression deformation at elevated temperatures, doi:10.4028/www.scientific.net/MSF.546-549.1061.

Humphreys, F. J., & Hatherly, M. (2004). *Recrystallization and related annealing phenomena* (2nd ed.). Oxford: Elsevier.

Hutchinson, B., Jonsson, S., & Ryde, L. (1989). On the kinetics of recrystallisation in cold worked metals. *Scripta Metallurgica*, *23*(5), 671–676. https://doi.org/10.1016/0036-9748(89)90510-3

Hutchinson, W. B., Besag, F. M. C., & Honess, C. V. (1973). The annealing behaviour of cold worked copper-25 at.% gold. *Acta Metallurgica*, *21*(12), 1685–1691.

Hutchinson, W. B., & Ray, R. K. (1979). Influence of phosphorus additions on annealing behaviour of cold-worked copper. *Metal Science*, *13*(3–4), 125–130. https://doi.org/10.1179/msc.1979.13.3-4.125

Jackson, I. (1976). Melting of the silica isotypes SiO_2, BeF_2 and GeO_2 at elevated pressures. *Physics and Chemistry of the Earth, Part A: Solid Earth and Geodesy*, *13*, 218–231.

Jessell, M. W., Siebert, E., Bons, P., Evans, L., & Piazolo, S. (2005). A new type of numerical experiment on the spatial and temporal patterns of localization of deformation in a material with a coupling of grain size and rheology. *Earth and Planetary Science Letters*, *239*(3–4), 309–326. https://doi.org/10.1016/J.EPSL.2005.03.030

Johnson, W. A., & Mehl, R. F. (1939). Reaction kinetics in processes of nucleation and growth. *Transactions of AIME*, *135*, 416–458.

Jonas, J. J., Quelennec, X., Jiang, L., & Martin, É. (2009). The Avrami kinetics of dynamic recrystallization. *Acta Materialia*, *57*(9), 2748–2756. https://doi.org/10.1016/j.actamat.2009.02.033

Karato, S. (1989). Grain growth kinetics in olivine aggregates. *Tectonophysics*, *168*(4), 255–273. https://doi.org/10.1016/0040-1951(89)90221-7

Kingery, W. D., Bowen, H. K., & Uhlmann, D. R. (1976). *Introduction to Ceramics* (1032 pp.). New York: Wiley.

Kolmogorov, A. N. (1937). On the statistical theory of crystallization of metals. *Izv. Akad. Nauk SSSR, Ser. Mat.*, *3*, 355–359.

Korenaga, J. (2005). Firm mantle plumes and the nature of the core–mantle boundary region. *Earth and Planetary Science Letters*, *232*(1–2), 29–37. https://doi.org/10.1016/J.EPSL.2005.01.016

Linckens, J., Herwegh, M., & Müntener, O. (2015). Small quantity but large effect—How minor phases control strain localization in upper mantle shear zones. *Tectonophysics*, *643*, 26–43. https://doi.org/10.1016/j.tecto.2014.12.008

Llana-Fúnez, S., Brodie, K. H., Rutter, E. H., & A. J. C. (2007). Experimental dehydration kinetics of serpentinite using pore volumometry. *Journal of Metamorphic Geology*, *25*(4), 423–438. https://doi.org/10.1111/j.1525-1314.2007.00703.x

Luton, M., & Sellars, C. (1969). Dynamic recrystallization in nickel and nickel-iron alloys during high temperature deformation. *Acta Metallurgica*, *17*(8), 1033–1043. https://doi.org/10.1016/0001-6160(69)90049-2

Medina, S. F., & Hernandez, C. A. (1996). Modelling of the dynamic recrystallization of austenite in low alloy and microalloyed steels. *Acta Materialia*, *44*(1), 165–171. https://doi.org/10.1016/1359-6454(95)00154-6

Montési, L. G. J., & Hirth, G. (2003). Grain size evolution and the rheology of ductile shear zones: From laboratory experiments to postseismic creep. *Earth and Planetary Science Letters*, *211*(1–2), 97–110. https://doi.org/10.1016/S0012-821X(03)00196-1

Mulyukova, E., & Bercovici, D. (2018). Collapse of passive margins by lithospheric damage and plunging grain size. *Earth and Planetary Science Letters*, *484*, 341–352.

Mulyukova, E., & Bercovici, D. (2019). A theoretical model for the evolution of microstructure in lithospheric shear zones. *Geophysical Journal International*, *216*(2), 803–819. https://doi.org/10.1093/gji/ggy467

Muto, J., Hirth, G., Heilbronner, R., & Tullis, J. (2011). Plastic anisotropy and fabric evolution in sheared and recrystallized quartz single crystals. *Journal of Geophysical Research*, *116*, B02206. https://doi.org/10.1029/2010JB007891

Olgaard, D. L., & Evans, B. (1988). Grain growth in synthetic marbles with added mica and water. *Contributions to Mineralogy and Petrology*, *100*(2), 246–260. https://doi.org/10.1007/BF00373591

Pennacchioni, G., Menegon, L., Leiss, B., Nestola, F., & Bromiley, G. (2010). Development of crystallographic preferred orientation and microstructure during plastic deformation of natural coarse-grained quartz veins. *Journal of Geophysical Research*, *115*, B12405. https://doi.org/10.1029/2010JB007674

Piazolo, S., Bons, P. D., Jessell, M. W., Evans, L., & Passchier, C. W. (2002). Dominance of microstructural processes and their effect on microstructural development: insights from numerical modelling of dynamic recrystallization. *Geological Society of London, Special Publication*, *200*(1), 149–170.

Pieri, M., Kunze, K., Burlini, L., Stretton, I., Olgaard, D. L., Burg, J.-P., & Wenk, H.-R. (2001). Texture development of calcite by deformation and dynamic recrystallization at 1000K during torsion experiments of marble to large strains. *Tectonophysics*, *330*(1-2), 119–140. https://doi.org/10.1016/S0040-1951(00)00225-0

Platt, J. P., & Behr, W. (2011). Grainsize evolution in ductile shear zones: Implications for strain localization and the strength of the lithosphere. *Journal of Structural Geology*, *33*(4), 537–550. https://doi.org/10.1016/J.JSG.2011.01.018

Platt, J. P., & De Bresser, J. H. P. (2017). Stress dependence of microstructures in experimentally deformed calcite. *Journal of Structural Geology*, *105*(October), 80–87. https://doi.org/10.1016/j.jsg.2017.10.012

Poirier, J. P. (1980), Shear localization and shear instability in materials in the ductile field, *Journal of Structural Geology*, *2*(1-2), 135–142. https://doi.org/10.1016/0191-8141(80)90043-7

Poirier, J. P. (1985). *Creep of crystals: High-temperature deformation processes in metals, ceramics and minerals*. New York: Cambridge University Press. https://doi.org/10.1017/CBO9780511564451

Poirier, J. P., & Guillopé, M. (1979). Deformation induced recrystallization of minerals. *Bulletin de Mineralogie*, *102*(2), 67–74. https://doi.org/10.3406/bulmi.1979.7256

Poliak, E. I., & Jonas, J. J. (1996). A one-parameter approach to determining the critical conditions for the initiation of dynamic recrystallization. *Acta Materialia*, *44*(1), 127–136. https://doi.org/10.1016/1359-6454(95)00146-7

Presnall, D. C. (1995). Phase diagrams of Earth-forming minerals. In *Mineral physics and crystallography: A handbook of physical constants* (pp. 248–268).

Qi, C., Goldsby, D. L., & Prior, D. J. (2017). The down-stress transition from cluster to cone fabrics in experimentally deformed ice. *Earth and Planetary Science Letters*, *471*, 136–147. https://doi.org/10.1016/j.epsl.2017.05.008

Ranganathan, S., & Von Heimendahl, M. (1981). The three activation energies with isothermal transformations: Applications to metallic glasses. *Journal of Materials Science*, *16*(9), 2401–2404. https://doi.org/10.1007/BF01113575

Riedel, M. R., & Karato, S.-I. (1996). Microstructural development during nucleation and growth. *Geophysical Journal International*, *125*(2), 397–414. https://doi.org/10.1111/j.1365-246X.1996.tb00007.x

Roberts, W., Boden, H., & Ahlblom, B. (1979). Dynamic recrystallization kinetics. *Metal Science*, *13*(3–4), 195–205. https://doi.org/10.1179/msc.1979.13.3-4.195

Rozel, A. (2012). Impact of grain size on the convection of terrestrial planets. *Geochemistry, Geophysics, Geosystems*, *13*, Q10020. https://doi.org/10.1029/2012GC004282

Rozel, A., Ricard, Y., & Bercovici, D. (2011). A thermodynamically self-consistent damage equation for grain size evolution during dynamic recrystallization. *Geophysical Journal International*, *184*(2), 719–728. https://doi.org/10.1111/j.1365-246X.2010.04875.x

Rutter, E. H. (1999). On the relationship between the formation of shear zones and the form of the flow law for rocks undergoing dynamic recrystallization. *Tectonophysics*, *303*(1–4), 147–158. https://doi.org/10.1016/S0040-1951(98)00261-3

Rutter, E. H., & Brodie, K. H. (1988). The role of tectonic grain size reduction in the rheological stratification of the lithosphere. *Geologische Rundschau*, *77*(1), 295–307. https://doi.org/10.1007/BF01848691

Sakai, T. (1989). Dynamic recrystallization of metallic materials. In S. Karato & M. Toriumi (Eds.), *Rheology of solids and of the Earth* (pp. 284–307). Oxford: Oxford University Press.

Shigematsu, N. (1999). Dynamic recrystallization in deformed plagioclase during progressive shear deformation. *Tectonophysics*, *305*(4), 437–452. https://doi.org/10.1016/S0040-1951(99)00039-6

Shigematsu, N., Fujimoto, K., Ohtani, T., Shibazaki, B., Tomita, T., Tanaka, H., & Miyashita, Y. (2009). Localisation of plastic flow in the mid-crust along a crustal-scale fault: Insight from the Hatagawa fault zone, NE Japan. *Journal of Structural Geology*, *31*(6), 601–614. https://doi.org/10.1016/J.JSG.2009.04.004

Shigematsu, N., & Tanaka, H. (2000). Dislocation creep of fine-grained recrystallized plagioclase under low-temperature conditions. *Journal of Structural Geology*, *22*(1), 65–79. https://doi.org/10.1016/S0191-8141(99)00132-7

Shimizu, I. (2008). Theories and applicability of grain size piezometers: The role of dynamic recrystallization mechanisms. *Journal of Structural Geology*, *30*(7), 899–917. https://doi.org/10.1016/j.jsg.2008.03.004

Skemer, P., & Karato, S. (2008). Sheared lherzolite xenoliths revisited. *Journal of Geophysical Research*, *113*, B07205. https://doi.org/10.1029/2007JB005286

Skemer, P., & Karato, S.-I. (2007). Effects of solute segregation on the grain-growth kinetics of orthopyroxene with implications for the deformation of the upper mantle. *Physics of the Earth and Planetary Interiors*, *164*(3-4), 186–196. https://doi.org/10.1016/j.pepi.2007.06.011

Skemer, P., Sundberg, M., Hirth, G., & Cooper, R. (2011). Torsion experiments on coarse-grained dunite: implications for microstructural evolution when diffusion creep is suppressed. *Geological Society of London, Special Publication*, *360*(1), 211–223. https://doi.org/10.1144/SP360.12

Somerday, M., & Humphreys, F. J. (2003). Recrystallisation behaviour of supersaturated Al–Mn alloys Part 2—Al–0.3 wt-%Mn. *Materials Science and Technology*, *19*(1), 30–35. https://doi.org/10.1179/026708303225008626

Stipp, M., Stünitz, H., Heilbronner, R., & Schmid, S. M. (2002). Dynamic recrystallization of quartz: Correlation between natural and experimental conditions. *Geological Society of London, Special Publication*, *200*(1), 171–190. https://doi.org/10.1144/GSL.SP.2001.200.01.11

Stormer, J. C. Jr. (1975). Practical two-feldspar geothermometer. *American Mineralogist (United States)*, *60*, 7–8.

Stüwe, H. P., Padilha, A. F., & Siciliano, F. (2002). Competition between recovery and recrystallization. *Materials Science and Engineering A*, *333*(1–2), 361–367. https://doi.org/10.1016/S0921-5093(01)01860-3

Suito, K., Namba, J., Horikawa, T., Taniguchi, Y., Sakurai, N., Kobayashi, M., et al. (2001). Phase relations of $CaCO_3$ at high pressure and high temperature. *American Mineralogist*, *86*(9), 997–1002. https://doi.org/10.2138/am-2001-8-906

Ter Heege, J. H., De Bresser, J. H. P., & Spiers, C. J. (2002). The influence of dynamic recrystallization on the grain size distribution and rheological behaviour of Carrara marble deformed in axial compression. *Geological Society of London, Special Publication*, *200*(1), 331–353. https://doi.org/10.1144/GSL.SP.2001.200.01.19

Thielmann, M., Rozel, A., Kaus, B. J. P., & Ricard, Y. (2015). Intermediate-depth earthquake generation and shear zone formation caused by grain size reduction and shear heating. *Geology*, *43*(9), 791–794. https://doi.org/10.1130/G36864.1

Tokle, L., Hirth, G., & Behr, W. M. (2019). Flow laws and fabric transitions in wet quartzite. *Earth and Planetary Science Letters*, *505*, 152–161. https://doi.org/10.1016/J.EPSL.2018.10.017

Tullis, J., & Yund, R. A. (1982). Grain growth kinetics of quartz and calcite aggregates. *Journal of Geology*, *90*(3), 301–318. https://doi.org/10.1086/628681

Tullis, J., & Yund, R. A. (1985). Dynamic recrystallization of feldspar: A mechanism for ductile shear zone formation. *Geology*, *13*(4), 238. https://doi.org/10.1130/0091-7613(1985)13<238:DROFAM>2.0.CO;2

Urai, J. L. (1987). Development of microstructure during deformation of carnallite and bischofite in transmitted light. *Tectonophysics*, *135*(1–3), 251–263. https://doi.org/10.1016/0040-1951(87)90166-1

Urai, J. L., Means, W. D., & Lister, G. S. (1986). Dynamic recrystallization of minerals (pp. 161–199).

Valcke, S. L. A., De Bresser, J. H. P., Pennock, G. M., & Drury, M. R. (2015). Influence of deformation conditions on the development of heterogeneous recrystallization microstructures in experimentally deformed Carrara marble. *Geological Society of London, Special Publication*, *409*(1), 175–200.

Van der Wal, D., Chopra, P., Drury, M., & Gerald, J. F. (1993). Relationships between dynamically recrystallized grain size and deformation conditions in experimentally deformed olivine rocks. *Geophysical Research Letters*, *20*(14), 1479–1482. https://doi.org/10.1029/93GL01382

Vaughan, M. J., Prior, D. J., Jefferd, M., Brantut, N., Mitchell, T. M., & Seidemann, M. (2017). Insights into anisotropy development and weakening of ice from in situ P wave velocity monitoring during laboratory creep. *Journal of Geophysical Research: Solid Earth*, *122*, 7076–7089. https://doi.org/10.1002/2017JB013964

Wang, J., Iwahashi, Y., Horita, Z., Furukawa, M., Nemoto, M., Valiev, R. Z., & Langdon, T. G. (1996). An investigation of microstructural stability in an AlMg alloy with submicrometer grain size. *Acta Materialia*, *44*(7), 2973–2982. https://doi.org/10.1016/1359-6454(95)00395-9

Warren, J. M., & Hirth, G. (2006). Grain size sensitive deformation mechanisms in naturally deformed peridotites. *Earth and Planetary Science Letters*, *248*(1–2), 438–450. https://doi.org/10.1016/j.epsl.2006.06.006

Wenk, H.-R., Canova, G., Bréchet, Y., & Flandin, L. (1997). A deformation-based model for recrystallization of anisotropic materials. *Acta Materialia*, *45*(8), 3283–3296. https://doi.org/10.1016/S1359-6454(96)00409-0

White, S. (1977). Geological significance of recovery and recrystallization processes in quartz. *Tectonophysics*, *39*(1-3), 143–170. https://doi.org/10.1016/0040-1951(77)90093-2

White, S. (1979). Grain and sub-grain size variations across a mylonite zone. *Contributions to Mineralogy and Petrology*, *70*(2), 193–202. https://doi.org/10.1007/BF00374448

White, S. H., Burrows, S. E., Carreras, J., Shaw, N. D., & Humphreys, F. J. (1980). On mylonites in ductile shear zones. *Journal of Structural Geology*, *2*(1-2), 175–187. https://doi.org/10.1016/0191-8141(80)90048-6

Whitney, J. A., & Stormer, J. C. Jr. (1977). Distribution of NaAlSi3O8 between coexisting microcline and plagioclase and its effect of geothermometric calculations. *American Mineralogist (United States)*, *62*(7/8), 687–691.

Woldt, E. (1992). The relationship between isothermal and non-isothermal description of Johnson-Mehl-Avrami-Kolmogorov kinetics. *Journal of Physics and Chemistry of Solids*, *53*(4), 521–527. https://doi.org/10.1016/0022-3697(92)90096-V

Wray, P. J. (1975). Onset of recrystallization during the tensile deformation of austenitic iron at intermediate strain rates. *Metallurgical Transactions A*, *6*(6), 1197–1203. https://doi.org/10.1007/BF02658529

Xia, H., & Platt, J. P. (2018). Quartz grainsize evolution during dynamic recrystallization across a natural shear zone boundary. *Journal of Structural Geology*, *109*, 120–126. https://doi.org/10.1016/J.JSG.2018.01.007

Yoshino, T., & Yamazaki, D. (2007). Grain growth kinetics of CaIrO3 perovskite and post-perovskite, with implications for rheology of D″ layer. *Earth and Planetary Science Letters*, *255*(3–4), 485–493. https://doi.org/10.1016/J.EPSL.2007.01.010